Development/Plasticity/Repair

# 12-Lipoxygenase Regulates Hippocampal Long-Term Potentiation by Modulating L-Type $Ca^{2+}$ Channels

**Anthony J. DeCostanzo,[2] Iryna Voloshyna,[2] Zev B. Rosen,[1] Steven J. Feinmark,[2,4] and Steven A. Siegelbaum[1,2,3]**

Departments of [1]Neuroscience and [2]Pharmacology, [3]Howard Hughes Medical Institute, and [4]Center for Molecular Therapeutics, Columbia University Medical Center, New York, New York 10032

**Although long-term potentiation (LTP) has been intensively studied, there is disagreement as to which molecules mediate and modulate LTP. This is partly attributable to the presence of mechanistically distinct forms of LTP that are induced by different patterns of stimulation and that depend on distinct $Ca^{2+}$ sources. Here, we report a novel role for the arachidonic acid-metabolizing enzyme 12-lipoxygenase (12-LO) in LTP at CA3–CA1 hippocampal synapses that is dependent on the pattern of tetanic stimulation. We find that 12-LO activity is required for the induction of LTP in response to a theta burst stimulation protocol that depends on $Ca^{2+}$ influx through both NMDA receptors and L-type voltage-gated $Ca^{2+}$ channels. In contrast, LTP induced by 100 Hz tetanic stimulation, which requires $Ca^{2+}$ influx through NMDA receptors but not L-type channels, does not require 12-LO. We find that 12-LO regulates LTP by enhancing postsynaptic somatodendritic $Ca^{2+}$ influx through L-type channels during theta burst stimulation, an action exerted via 12(*S*)-HPETE [12(*S*)-hydroperoxyeicosa-5*Z*,8*Z*,10*E*,14*Z*-tetraenoic acid], a downstream metabolite of 12-LO. These results help define the role of a long-disputed signaling enzyme in LTP.**

## Introduction

Distinct cellular pathways for elevating $Ca^{2+}$ are activated by neural activity in a stimulus pattern-dependent manner, such that different patterns of presynaptic activity recruit distinct postsynaptic $Ca^{2+}$ sources (Collingridge et al., 1983; Johnston et al., 1992; Cavuş and Teyler, 1996; Collingridge, 2003; Malenka and Bear, 2004; Striessnig et al., 2006). In turn, these different $Ca^{2+}$ sources may recruit distinct $Ca^{2+}$-dependent signaling modules to induce specific forms of long-term synaptic plasticity.

At CA3–CA1 synapses, two fundamental $Ca^{2+}$ sources have been found to participate in distinct forms of long-term potentiation (LTP) induced by different patterns of synaptic activity, NMDA receptors and L-type voltage-gated $Ca^{2+}$ channels (LTCCs) (Grover and Teyler, 1990). Thus, whereas LTP induced by 100 Hz tetanic stimulation depends primarily on $Ca^{2+}$ influx through NMDA receptors (Collingridge et al., 1983), LTP induced by 200 Hz tetanic stimulation (Grover and Teyler, 1990; Zakharenko et al., 2001) or prolonged theta burst stimulation (TBS) requires $Ca^{2+}$ influx through both NMDA receptors (NMDARs) and LTCCs (Morgan and Teyler, 2001). These two forms of plasticity also differ in their dependence on second messenger cascades, with 100 Hz LTP requiring serine/threonine kinases and LTCC-dependent LTP requiring tyrosine kinases (Morgan and Teyler, 1999, 2001).

There is an expanding literature on the role of arachidonic acid-derived lipids in synaptic plasticity, most recently focusing on the endocannabinoid system (Chevaleyre et al., 2006). The initial suggestion that 12-lipoxygenase (12-LO) could play a role in synaptic plasticity came from experiments in *Aplysia* sensory neurons demonstrating that 12-LO metabolites of arachidonic acid mediate the activation of the S-type $K^+$ channel and presynaptic inhibition of glutamate release in response to the neuropeptide FMRFamide (Piomelli et al., 1987a,b; Buttner et al., 1989). Support for a role for 12-LO metabolites in LTP came from the finding that arachidonic acid, the substrate of 12-LO, can facilitate induction of LTP (Williams and Bliss, 1989; Williams et al., 1989; O'Dell et al., 1991). However, evidence for the role of 12-LO in LTP has been controversial (O'Dell et al., 1991) and hampered by lack of selective inhibitors and genetically engineered mice. Renewed interest in the 12-LO pathway comes from two more recent studies demonstrating a role for 12-LO metabolites in metabotropic glutamate receptor (mGluR)-dependent long-term depression (LTD) at neonatal CA3–CA1 synapses (Feinmark et al., 2003) and LTD at excitatory synapses onto CA1 inhibitory interneurons (Gibson et al., 2008).

Here, for the first time, we compare at hippocampal CA3–CA1 synapses the role of 12-LO in distinct forms of LTP that are induced by different tetanic stimulation protocols using a genetic knock-out of the brain isoform of 12-LO (Sun and Funk, 1996) and a selective pharmacological inhibitor of 12-LO. We find a specific role for 12-LO in LTCC-dependent LTP induced by TBS but not in NMDAR-dependent LTP induced by 100 Hz tetanic stimulation. Furthermore, our results indicate that constitutive activity of 12-LO, acting through the production of the arachidonic acid metabolite 12(*S*)-hydroperoxyeicosa-5*Z*,8*Z*,10*E*,14*Z*-tetraenoic acid [12(*S*)-HPETE], is required for normal LTCC function, thus enabling sufficient $Ca^{2+}$ influx into the CA1

Received May 7, 2009; revised Oct. 7, 2009; accepted Dec. 11, 2009.

This work was supported by National Institutes of Health Grant MH045923. We thank Robert Hawkins, Bina Santoro, David Tsay, Joshua Dudman, Yelena Gor, and Rebecca Piskorowski for their experimental insights.

This work is dedicated to the memory of our colleague and good friend Dr. James H. Schwartz, whose insight inspired our study of the role of 12-LO in the nervous system.

Correspondence should be addressed to Anthony J. DeCostanzo, Columbia University Medical Center, 1051 Riverside Drive, Room 724, New York, NY 10032. E-mail: ajd2003@columbia.edu.

DOI:10.1523/JNEUROSCI.2168-09.2010

 0270-6474/10/301822-10$15.00/0

pyramidal neurons in response to TBS to induce LTP. As LTCC-dependent plasticity is critical for certain aspects of hippocampal-dependent learning (Borroni et al., 2000; Moosmang et al., 2005), 12-LO is likely to function as a key modulator of learning and memory.

## Materials and Methods

*Hippocampal slice preparation.* Transverse hippocampal slices were prepared from 6- to 8-week-old 12-LO $^{-/-}$ or 12-LO $^{+/+}$ mice littermates obtained by backcrossing the original 12-LO knock-out line (on a mixed C57BL/6 × 129 Sv background) (Sun and Funk, 1996) >10 times onto the C57BL/6 strain. These mice lack the neuronal (leukocyte) isoform of 12-LO, the major isoform expressed in brain, leading to a decrease in levels of 12-LO activity in hippocampal slices to approximately one-third that seen in wild-type mice (Feinmark et al., 2003). Where indicated, wild-type mice from The Jackson Laboratory were used. After cervical dislocation and rapid decapitation, the brain was dissected and placed in cold (4°C) dissection–artificial CSF (ACSF) for 5 min to allow the temperature to equilibrate. The dissection-ACSF had the following composition (in mM): 124 choline-Cl, 1.2 $NaH_2PO_4$, 4.3 KCl, 25 $NaHCO_3$, 10 glucose, 0.4 $CaCl_2$, 6 $MgCl_2$. While at 4°C, the hippocampus was dissected out of the brain and glued to an agar block, with the CA1 region facing outward. Three hundred-micrometer-thick sections were cut with a Vibroslice sectioning system (Campden) and transferred to a storage container filled with standard ACSF at 25°C.

*Field and whole-cell current-clamp recordings and solutions.* Slices were incubated for at least 1.5 h in standard ACSF before recording. The standard ACSF had the following composition (in mM): 124 NaCl, 1.2 $NaH_2PO_4$, 4.3 KCl, 25 $NaHCO_3$, 10 glucose, 2 $CaCl_2$, 2 $MgCl_2$. After 1.5–6 h of incubation, slices were transferred into a submerged chamber for recording. For field recordings, slices were perfused with standard ACSF, and a 3–5 MΩ extracellular glass recording pipette filled with ACSF was placed in stratum radiatum of the CA1 subfield. All experiments were performed at 25–26.5°C. For all experiments requiring presynaptic stimulation, a tungsten stimulating electrode was placed in stratum radiatum of CA3 to stimulate Schaffer collateral axons using an A365 constant-current stimulus isolation unit (World Precision Instruments). Baseline stimulation consisted of 0.1 ms current pulses given at 0.033 Hz at 50% maximal stimulation intensity. The synaptic input–output relationship was determined by increasing stimulation intensity from 0 to 250 μA in 50 μA increments and recording the resultant field EPSPs (fEPSPs). The 100 Hz LTP induction protocol consisted of four 1 s, 100 Hz stimulus trains separated by a 20 s interval between trains. The TBS induction protocol consisted of six trains of five bursts of stimulation, using four pulses per burst. Trains were separated by 10 s, bursts were separated by 200 ms (theta rhythm), and the four pulses within a burst were delivered at 100 Hz (Morgan and Teyler, 2001; Zakharenko et al., 2003). TBS-LTP experiments in the presence of D-APV (Tocris) used a stimulus intensity of 75% maximum stimulation intensity during the TBS trains to generate an LTP that was NMDAR independent and LTCC dependent (Morgan and Teyler, 2001). Unless indicated otherwise, LTP was measured as the mean of fEPSPs from 55-50 minutes after induction. 12(*S*)-HPETE was synthesized from partially purified porcine leukocyte 12-lipoxygeanse prepared by a slight modification of an established method (Kitamura et al., 1987). 12(*S*)-HPETE was purified as the free acid by preparative normal-phase HPLC and quantified by UV absorbance ($\lambda_{max}$ = 237 nm and $\varepsilon$ = 23,000 $M^{-1} \cdot cm^{-1}$). We thank Dr. Joseph Cornicelli of Pfizer for providing PD146176.

For whole-cell current-clamp recordings, a 3–5 MΩ recording electrode was filled with artificial internal solution containing the following (in mM): 130 $KMeSO_4$, 10 KCl, 10 HEPES, 4 NaCl, 0.4 Fluo-4, 4 MgATP, 0.3 $Na_2GTP$, and 10 phosphocreatine. Both series resistance and capacitance were compensated. Capacitance was well compensated at 7.8–8.2 pF. Series resistance with capacitance compensated was between 15 and 30 MΩ. Only data from cells in which resting potential was negative to −60 mV were used for analysis.

*$Ca^{2+}$ current voltage-clamp recordings.* Artificial internal solution was prepared with the following (in mM): 130 $CsMeSO_4$, 10 HEPES, 4 MgATP, 0.3 $Na_2GTP$, 12 $Na_2$-phosphocreatine, 1 CaOH, 10 EGTA, and then pH was adjusted with CsOH (~8 mM final). A 3–5 MΩ patch electrode filled with internal solution was used to record from CA1 pyramidal neurons in slices perfused with modified ACSF containing the following (in mM): 99 NaCl, 1.2 $NaH_2PO_4$, 4.3 KCl, 25 $NaHCO_3$, 10 glucose, 2 $CaCl_2$, 2 $MgCl_2$, 20 tetraethylammonium chloride, and 5 4-aminopyridine. The 10 mV voltage steps were given from a holding potential of −40 mV. Peak inward current for each step was measured to obtain current–voltage curves.

*Two-photon $Ca^{2+}$ imaging.* $Ca^{2+}$ dye was loaded into CA1 cells under whole-cell current-clamp conditions with patch pipettes filled with 0 EGTA internal solution supplemented with 0.4 mM Fluo-4 ($K_d$ = 345 nM; Invitrogen). After 12 min of whole-cell recording to load the dye, the pipette was slowly removed from the surface of the cell until a >2 GΩ reseal was observed at the tip of the electrode. This procedure avoided problems associated with "washing out" of signaling molecules associated with prolonged whole-cell recordings (Lamsa et al., 2005). $Ca^{2+}$ imaging commenced 20 min after resealing of the cell membrane. Stimulation consisted of a single train of TBS, five bursts of four pulses at 100 Hz, with 200 ms between bursts. The green (Fluo-4) signal was measured for the full 4 s, providing a 500 ms baseline before the start of the first burst of TBS. Synaptic stimulation intensity was adjusted so that a single burst of four pulses at 100 Hz elicited a single postsynaptic action potential under current clamp. This procedure ensured that the measured $Ca^{2+}$ transient represents the response to a single spike per burst for both wild-type and 12-LO knock-out mice. All $Ca^{2+}$ imaging experiments were performed in the presence of 50 μM D-APV.

Two-photon imaging was performed with a Bio-Rad Radiance 2100 MP (Zeiss), powered by a tunable MaiTai titanium/sapphire pulsed laser (Spectra Physics) tuned to 800 nm. The green Fluo-4 signal was detected as an epifluorescence signal through a 60×, 1.1 numerical aperture objective (Olympus) by custom gallium arsenide phosphide (GaAsP) detectors (Multiphoton Peripherals). Four second line scans were performed at 500 Hz across the proximal dendrite just at the juncture with the soma. Using LaserSharp software (Bio-Rad), line scans were triggered by a stimulation protocol from pCLAMP8.0. The green fluorescence signal was then processed accordingly. Each line of the 500 Hz, 4 s scan was averaged to give a single point, representing a 2 ms bin. These 4 s traces were then boxcar averaged with a sliding window of 20 ms (10 data points). Baseline fluorescence was taken as the mean of the first 20 ms of green signal. The $Ca^{2+}$ response to synaptically induced action potentials was calculated as the percentage change in fluorescence over baseline fluorescence ($\%\Delta F/F_0$) = 100% × $(F - F_0)/F_0$.

*Data acquisition and analysis.* For field stimulation, an A365 constant-current stimulus isolator (World Precision Instruments) was triggered with TTL pulses from acquisition software. For field recordings, a HEKA EPC9 analog–digital–analog converter was used with both stimulation and acquisition controlled by Pulse 8.53 software (HEKA Instruments). An Axoclamp 200A amplifier (Molecular Devices) was used for field current-clamp recordings of fEPSPs. Whole-cell current-clamp recordings were made with a Multiclamp 700A amplifier (Molecular Devices) controlled with pCLAMP8.0 (Molecular Devices). Traces were filtered with a low-pass 1 kHz digital filter (fast Fourier transform). For spike statistics including threshold, afterhyperpolarization potential, spike count, and instantaneous spike rate, traces were scanned for spikes using the pCLAMP8.0 spike template search. Spike template matches were confirmed by eye. Mean statistics were then computed and analyzed in Microsoft Excel (Microsoft) or in IGOR Pro (WaveMetrics). Significance levels are indicated with asterisks to indicate $p$ values of $< 0.05$ (*), $< 0.01$ (**), and $< 0.001$ (***).

## Results

### Stimulus pattern-dependent requirement for 12-LO in the induction of LTP

We first examined the importance of 12-LO in NMDAR-dependent LTP induced by 100 Hz tetanic stimulation. One hundred hertz LTP was compared between mice with a deletion of the neuronal (leukocyte) isoform of 12-LO (12-LO $^{-/-}$) and their

wild-type (12-LO $^{+/+}$) littermates (Fig. 1*A*). A comparison of the time course of LTP between genotypes at 4, 30, and 60 min after induction revealed no significant difference between genotypes. Thus, in 12-LO $^{+/+}$ mice, the 100 Hz tetanic stimulation enhanced the fEPSP slope to 271 ± 33, 207 ± 33, and 183 ± 21% of its initial value at 4, 30, and 60 min after the tetanus. We observed similar increases of the fEPSP in 12-LO $^{-/-}$ mice to 251 ± 14, 232 ± 16, and 205 ± 12% of initial fEPSP size at the corresponding time points ($p = 0.7815$ between genotypes with repeated-measures ANOVA). The lack of change in 100 Hz LTP is similar to results of a previous study in 12-LO KO mice on a different genetic background (Feinmark et al., 2003).

In contrast to the lack of change in 100 Hz LTP, the 12-LO $^{-/-}$ mice showed a significant impairment in the magnitude of NMDAR-dependent and LTCC-dependent LTP induced by TBS, relative to the magnitude of TBS-LTP in wild-type littermates (Fig. 1*B*). In 12-LO $^{+/+}$ mice TBS enhanced the fEPSP to 238 ± 17, 202 ± 15, and 187 ± 13% of its initial value measured at 4, 30, and 60 min after the induction protocol. In contrast, in 12-LO $^{-/-}$ mice, TBS produced a smaller enhancement to 185 ± 13, 167 ± 11, and 157 ± 10% of the initial fEPSP measured at the corresponding time points ($p = 0.048$ between genotypes with repeated-measures ANOVA). This defect in TBS-LTP was not attributable to altered basal synaptic transmission as both the fEPSP input–output relationship and paired-pulse ratio, a measure of presynaptic function, were similar between genotypes (Fig. 1*C*, *D*).

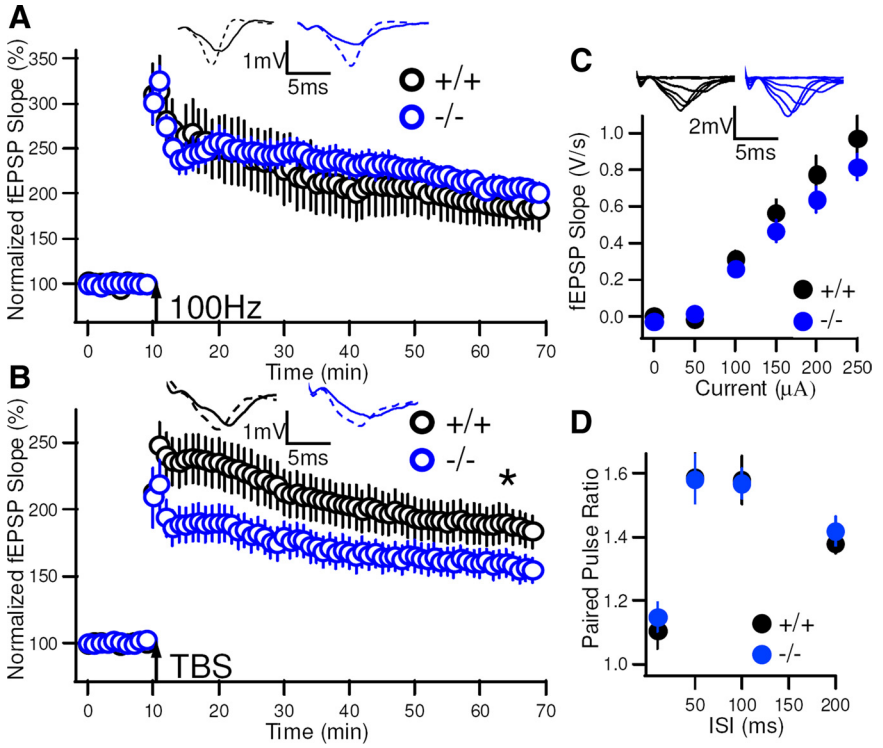


**Figure 1.** Stimulus pattern-dependent deficit in LTP at CA3–CA1 synapses in 12-LO $^{-/-}$ mice. ***A***, Four trains of 1-s-long 100 Hz stimulation (arrow) produced a similar amount of LTP in 12-LO $^{+/+}$ (black) and 12-LO knock-out mice (blue), yielding 271 ± 33, 207 ± 33, and 183 ± 21% of baseline at 4, 30, and 60 min after the tetanus compared to 251 ± 14, 232 ± 16, and 205 ± 12% of initial fEPSP values in 12-LO $^{-/-}$ mice at corresponding time points ($p = 0.7815$ for between-genotype comparison with repeated-measures ANOVA). ***B***, TBS (arrow) elicited LTP that was significantly different between slices from 12-LO $^{+/+}$ (black) and 12-LO $^{-/-}$ (blue) mice, yielding 238 ± 17, 202 ± 15, and 187 ± 13% in 12-LO $^{+/+}$ mice versus 185 ± 13, 167 ± 11, and 157 ± 10% of the baseline fEPSP measured at 4, 30, and 60 min after induction ($p = 0.048$ with main effect of genotype with repeated-measures ANOVA). Insets for ***A*** and ***B*** show sample fEPSP traces before (solid line) and 60 min after (dashed line) LTP induction. ***C***, Basal synaptic transmission did not differ between 12-LO $^{+/+}$ (black) and 12-LO $^{-/-}$ (blue) mice. Input–output relationship plotting fEPSP slope versus stimulating current strength. The inset shows sample fEPSPs. Fifty percent of the maximal test stimulation yielded similar fEPSP slopes between genotypes ($p = 0.351$ with unpaired Student's *t* test), as did the maximum stimulation intensity ($p = 0.58$ with unpaired Student's *t* test). ***D***, Paired-pulse ratios (PPRs) were similar between genotypes. Pairs of stimuli were delivered at given interstimulus intervals. PPRs were obtained by dividing fEPSP slope in response to second pulse by fEPSP slope in response to first pulse. With unpaired Student's *t* test between genotypes at 10, 50, 100, and 200 ms interstimulus intervals, *p* values were 0.36, 0.85, 0.90, and 0.50, respectively. Error bars represent ±SEM. The asterisks indicate significance level.

### The NMDA receptor-independent component of LTP is selectively abolished in the absence of 12-LO activity

As 100 Hz LTP has been found to depend solely on $Ca^{2+}$ influx through NMDARs whereas TBS-LTP involves $Ca^{2+}$ influx through both NMDARs and LTCCs (Morgan and Teyler, 2001; Bliss et al., 2003; Zakharenko et al., 2003), we hypothesized that 12-LO may be selectively involved in the NMDAR-independent, LTCC-dependent component of TBS-LTP. To explore this idea, we examined the effects of 12-LO deletion on the NMDAR-independent component of TBS-LTP.

To isolate the NMDAR-independent component of TBS-LTP, we applied the theta burst stimulation protocol in the presence of the NMDAR antagonist D-APV (50 μM). Under these conditions, the tetanus induced a slowly developing component of LTP in wild-type (12-LO $^{+/+}$) mice (Fig. 2*A*). Sixty minutes after the TBS protocol, the fEPSP was enhanced to 129 ± 6.82% of its initial baseline value ($n = 9$). This NMDAR-independent component of LTP was completely abolished in slices from 12-LO $^{-/-}$ littermates, in which the TBS protocol induced an initial depression in the fEPSP, whose amplitude then returned to baseline values in 20–30 min. Sixty minutes after the TBS protocol, the fEPSP had fully returned to its initial value (100 ± 6.5% of baseline; $n = 9$), which was significantly smaller than the potentiation seen in wild-type mice ($p = 0.021$). Such results demonstrate the complete loss of the NMDAR-independent component of LTP after deletion of 12-LO.

To examine whether the deficit in NMDAR-independent LTP in the 12-LO knock-out mice could be attributable to a change in inhibitory synaptic transmission, we repeated the TBS protocol in the presence of gabazine and (2*S*)-3-[[(1*S*)-1-(3,4-dichlorophenyl) ethyl]amino-2-hydroxypropyl](phenylmethyl)phosphinic acid (CGP55845), antagonists of $GABA_A$ and $GABA_B$ receptors, respectively (Fig. 2*B*). In the presence of the GABA receptor blockers, TBS enhanced the fEPSP in the 12-LO $^{+/+}$ mice to 129 ± 15.7% ($n = 6$) of its initial value 60 min after the induction protocol, identical with the amount of NMDAR-independent LTP seen above with inhibition intact. Also similar to our results in the absence of GABA antagonists, TBS-LTP was absent in the 12-LO $^{-/-}$ mice when inhibition was blocked, with a small depression of the fEPSP present 60 min after the induction protocol (fEPSP size was 93 ± 6.2% of its initial value; $n = 9$; $p = 0.030$). These results suggest that 12-LO must exert its effects to enable the induction of TBS-LTP at some site in the

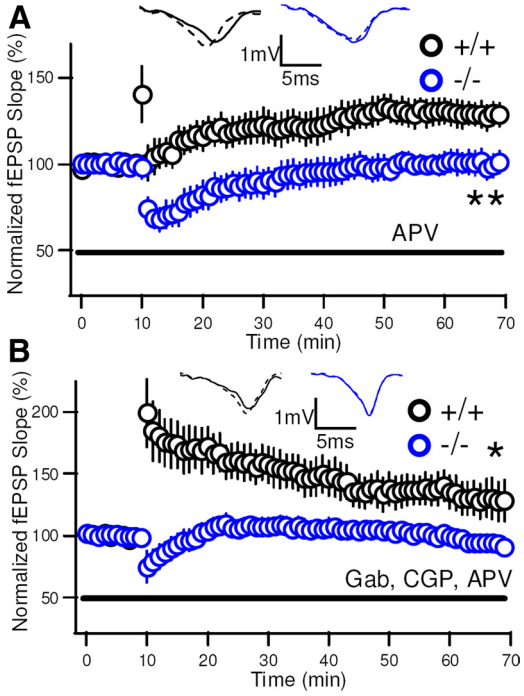


**Figure 2.** NMDAR-independent LTP is abolished in 12-LO $^{-/-}$ mice. ***A***, LTP was induced using TBS in slices from 12-LO $^{+/+}$ and 12-LO $^{-/-}$ mice in the presence of 50 $\mu$M D-APV to block NMDA receptors. Slices from 12-LO $^{+/+}$ mice (black) exhibited a potentiation of 129 $\pm$ 6.82% ($n = 9$) relative to baseline; slices from 12-LO $^{-/-}$ mice (blue) showed no potentiation, with fEPSP after TBS equal to 100 $\pm$ 6.50% of baseline ($n = 9$; $p = 0.021$, with ANOVA, Tukey's *post hoc*). Note transient depression seen in slices from 12-LO-deficient mice. ***B***, The effect of 12-LO deletion to inhibit NMDAR-independent LTP does not depend on inhibitory synaptic transmission. The protocol described in ***A*** was repeated in the presence of 2 $\mu$M gabazine (Gab), a $GABA_A$ receptor antagonist, and 4 $\mu$M CGP55845 (CGP), a $GABA_B$ receptor antagonist. In the presence of APV, Gab, and CGP, TBS enhanced the fEPSP to 129 $\pm$ 15.7% ($n = 6$; black) of baseline in 12-LO $^{+/+}$ mice but had no potentiating effect in 12-LO $^{-/-}$ mice, with fEPSP equal to 93 $\pm$ 6.15% ($n = 9$; blue) of baseline ($p = 0.030$, with unpaired Student's *t* test). The black horizontal bars indicate presence of drugs. Insets show sample fEPSP traces before (solid line) and 60 min after (dashed line) LTP induction. Error bars represent $\pm$SEM. The asterisks indicate significance level.

excitatory glutamatergic synaptic pathway, rather than through a modulation of inhibitory synaptic transmission.

Although blockade of inhibition had no effect on LTP measured 60 min after the TBS protocol, GABA receptor blockade did influence the early time course of synaptic plasticity, in both 12-LO $^{+/+}$ and 12-LO $^{-/-}$ mice. Thus, in wild-type mice, the GABA antagonists converted the slowly rising time course of NMDAR-independent TBS-LTP to a near instantaneous potentiation. In the 12-LO knock-out mice, the GABA receptor blockade decreased the magnitude of the early depression of the fEPSP after TBS and sped the recovery of the fEPSP to its initial baseline value. Both of these effects suggest that, in the presence of APV, TBS recruits a transient increase in feedforward inhibitory synaptic transmission that does not require 12-LO activity. Since the extent of TBS-LTP measured 60 min after its induction does not differ in the presence or absence of inhibitory synaptic transmission, we have limited our comparisons to this time frame.

### 12-LO is required for the L-type $Ca^{2+}$ channel-dependent component of TBS-LTP

As the NMDAR-independent component of TBS-LTP depends on $Ca^{2+}$ influx through L-type $Ca^{2+}$ channels (Morgan and Teyler, 2001; Zakharenko et al., 2003), our above results are consistent with the view that 12-LO is necessary for the LTCC of TBS-LTP. To explore this idea directly, we first confirmed that LTCCs do indeed contribute to TBS-LTP in wild-type (12-LO $^{+/+}$) mice. Indeed, we found that the magnitude of LTP was substantially reduced when the theta burst stimulation was applied with L-type channels blocked by 20 $\mu$M nitrendipine (Nitr) (Fig. 3*A*,*C*). Thus, whereas the TBS protocol normally enhanced the fEPSP to 190 $\pm$ 19.5% ($n = 7$) of its initial value (in the presence of 0.2% DMSO as a vehicle control), we observed only a 140 $\pm$ 12.0% ($n = 7$) potentiation when the TBS protocol was applied in the presence of Nitr ($p = 0.046$). In striking contrast, the residual TBS-LTP observed in slices from 12-LO $^{-/-}$ mice was insensitive to the blockade of L-type channels with Nitr (Fig. 3*B*,*C*). Thus, in the knock-out mice, the LTP induced by TBS enhanced the fEPSP in the presence of Nitr to 152 $\pm$ 16% of baseline, nearly identical with the enhancement observed in the absence of Nitr (156 $\pm$ 15.2% of its initial value; $p = 0.84$; $n = 7$ for both groups). This suggests that the LTCC-dependent contribution to TBS-LTP is fully abolished in the 12-LO $^{-/-}$ mice.

To explore further the relationship of the 12-LO-dependent and LTCC-dependent components of TBS-LTP, we next examined the effects of Nitr on TBS-LTP induced in the presence of D-APV, to compare the isolated NMDAR-independent component of TBS-LTP in wild-type versus 12-LO knock-out mice. We found that the NMDAR-independent component of TBS-LTP in wild-type mice was fully blocked when the TBS protocol was applied in the presence of Nitr (Fig. 3*D*,*F*). Thus, whereas delivery of the TBS protocol in the presence of 50 $\mu$M D-APV enhanced the fEPSP to 129 $\pm$ 6.8% ($n = 9$) of its initial level, application of the same TBS protocol in the combined presence of 50 $\mu$M D-APV and 20 $\mu$M Nitr caused a slight depression in the fEPSP to 90 $\pm$ 10% ($n = 3$) of its initial level ($p < 0.04$, relative to TBS-LTP in absence of Nitr; both measured 60 min after TBS). When measured 60 min after delivery of the tetanus in D-APV, TBS-LTP was fully blocked in the knock-out mouse, either in the absence or presence of nitrendipine (Fig. 3*E*,*F*) ($p = 0.66$). These results confirm that LTCCs are necessary for the NMDAR-independent and12-LO-dependent component of theta burst LTP. Interestingly, when we examined the effects of nitrendipine on the response to TBS in the 12-LO knock-out mice, we found that the $Ca^{2+}$ channel antagonist blocked the transient depression seen with TBS in the presence of D-APV (Fig. 3*E*).

To examine whether the defect in TBS-LTP on 12-LO deletion may be caused by some developmental change attributable to loss of this metabolic pathway, rather than a more acute involvement of 12-LO, we compared LTCC-dependent LTP in wild-type mice in the presence and absence of the 12-LO inhibitor, 6,11-dihydro[1]benzothiopyrano[4,3-b]indole (PD146176) (Fig. 4), which has been shown to be highly selective for the 12/15-lipoxygenase enzyme (Sendobry et al., 1997). Although PD146176 had no effect on baseline synaptic transmission (supplemental Fig. S3*A*, available at www.jneurosci.org as supplemental material), preincubation of hippocampal slices for 2 h in 10 $\mu$M PD146176 completely blocked LTCC-dependent LTP observed in the presence of D-APV. Thus, TBS enhanced the fEPSP to 138 $\pm$ 3.45% of its initial level in the absence of the 12-LO inhibitor. However, in the presence of PD146176, TBS led to a small depression of the fEPSP similar to the initial depression in 12-LO $^{-/-}$ mice, which eventually returned to 96.6 $\pm$ 6.37% of its baseline value ($p = 0.00048$). This suggests that 12-LO activity is required either during or immediately before the LTP induction protocol for the induction of LTCC-dependent LTP.

As a test of the specificity of the 12-LO inhibitor, we examined its effects on 100 Hz LTP, which was not affected by the genetic deletion of this enzyme. Incubation of slices with 10 μM PD146176 did not alter the magnitude of LTP induced by the 100 Hz tetanic stimulation (supplemental Fig. S1*B*, available at www.jneurosci.org as supplemental material), providing strong support for both the specificity of this agent and the selective involvement of 12-LO in LTCC-dependent LTP but not in NMDAR-dependent LTP.

### TBS-LTP depends on the 12-LO metabolite of arachidonic acid 12(*S*)-HPETE

12-LO converts arachidonic acid into 12(*S*)-HPETE, which is then rapidly reduced by tissue peroxidases to 12(*S*)-hydroxyeicosa-5*Z*,8*Z*,10*E*,14*Z*-tetraenoic acid [12(*S*)-HETE]. We therefore next investigated whether these metabolites are likely to contribute to the induction of TBS-LTP by examining whether either compound was able to rescue LTP when 12-LO activity is blocked with PD146176.

To investigate this question, we applied 10 μM PD146176 to slices from wild-type mice in the presence of D-APV to block the 12-LO/LTCC-dependent component of TBS-LTP (Fig. 5*A*,*B*). As described above (Fig. 4), application of the theta burst stimulation protocol in the presence of D-APV and PD146176 failed to evoke LTP, with the fEPSP remaining at 98.7 ± 10.4% of its baseline value ($n = 6$). We next applied 250 nM 12(*S*)-HPETE to slices in the presence of D-APV and PD146176 20 min before the TBS protocol. Although 12(*S*)-HPETE did not affect baseline synaptic transmission (supplemental Fig. S3*B*, available at www.jneurosci.org as supplemental material), under these conditions, 12(*S*)-HPETE fully rescued LTP, with the TBS protocol now producing a normal-sized enhancement of the fEPSP to 126.3 ± 3.96% of its initial level ($n = 10$; $p = 0.015$). Because 12(*S*)-HPETE on its own did not alter the fEPSP, we conclude that this metabolite is necessary but not sufficient for the induction of TBS-LTP.

We next examined whether 12(*S*)-HETE, the downstream metabolite of 12(*S*)-HPETE, was also capable of rescuing LTP. However, application of 250 nM 12(*S*)-HETE to slices bathed in D-APV and PD146176 failed to rescue TBS-LTP. Thus, application of the TBS protocol in the presence of 12(*S*)-HETE plus D-APV and PD146176 failed to enhance the fEPSP, which remained at 97.5 ± 4.7% of its baseline value ($n = 7$; $p = 0.99$). Thus, either 12(*S*)-HPETE itself or an active metabolite distinct from 12(*S*)-HETE is likely to participate in the induction of TBS-LTP.

To determine whether the 12(*S*)-HPETE acts upstream or downstream of LTCC activation during the TBS protocol, we repeated the 12(*S*)-HPETE rescue experiment, but in the added presence of Nitr to block the LTCCs. In contrast to the rescue of TBS-LTP seen when 12(*S*)-HPETE was applied in the presence of D-APV and PD146176, the lipid metabolite failed to rescue LTP when Nitr was also present in the bath solution. Thus, after delivery of the TBS protocol in the presence of 12(*S*)-HPETE, PD146176, D-APV, and Nitr, the fEPSP remained unchanged, equal to 94.7 ± 5.9% ($n = 5$) of its baseline value when measured 60 min after the induction protocol. This is in contrast to the enhancement in the fEPSP to 126.3 ± 3.96% ($n = 10$) of baseline observed above in the absence of Nitr ($p = 0.008$).

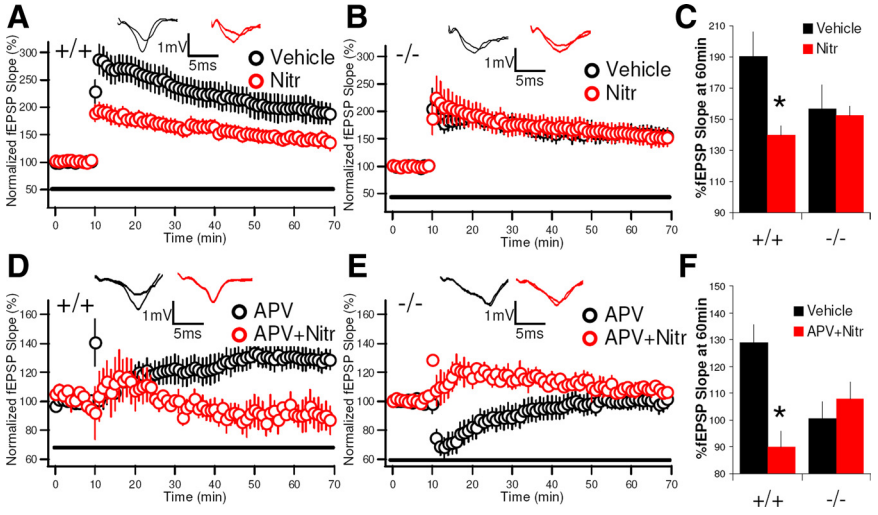


**Figure 3.** L-type $Ca^{2+}$ channel-dependent LTP is selectively abolished in 12-LO $^{-/-}$ mice. ***A–C***, LTP was induced using TBS in slices from 12-LO $^{+/+}$ and 12-LO $^{-/-}$ mice in the presence or absence of 20 μM Nitr to determine the proportion of potentiation that corresponded to LTCC-dependent LTP. ***A***, ***C***, In 12-LO $^{+/+}$ mice, TBS enhanced fEPSP to 190 ± 19.5% ($n = 7$) of baseline in the absence of Nitr (black) versus 140 ± 12.0% ($n = 7$) in presence of Nitr (red; $p = 0.046$). ***B***, ***C***, However, in knock-out (−/−) mice, TBS enhanced fEPSP to 156 ± 15.2% ($n = 7$) and 152 ± 16% ($n = 7$) of baseline values in the absence (black) and presence (red) of Nitr, respectively ($p = 0.84$). Comparisons were made with Student's *t* test. ***D–F***, The same protocol described above was used, but in the continuous presence of D-APV to isolate the LTCC-dependent component of LTP. The presence of D-APV revealed the NMDAR-independent component of TBS-LTP, which was fully blocked by Nitr. ***D***, ***F***, In 12-LO $^{+/+}$ mice, TBS enhanced the fEPSP to 129 ± 6.8% ($n = 9$) and 90 ± 10.0% ($n = 3$) of its initial value in the absence (black) and presence (red) of Nitr, respectively ($p = 0.026$). ***E***, ***F***, In slices from 12-LO $^{-/-}$ mice, the fEPSP was unchanged by TBS, either in the absence (black; fEPSP equal to 100 ± 6.5% of baseline; $n = 9$) or in the presence of Nitr (red; fEPSP equal to 108 ± 3.2% of baseline; $n = 3$; $p = 0.931$). Comparisons were made with ANOVA, Tukey's *post hoc* comparison. LTP data from wild-type mice in presence of D-APV and absence of Nitr in ***D*** and ***F*** are replotted from Figure 2. The bar graphs show change in fEPSP slope 60 min after TBS stimulation, measured as means of the last five data points (5 min). Insets for ***A***, ***B***, ***D***, and ***E*** show sample fEPSP traces before (solid line) and 60 min after (dashed line) LTP induction. Error bars represent ±SEM. The asterisks indicate significance level.

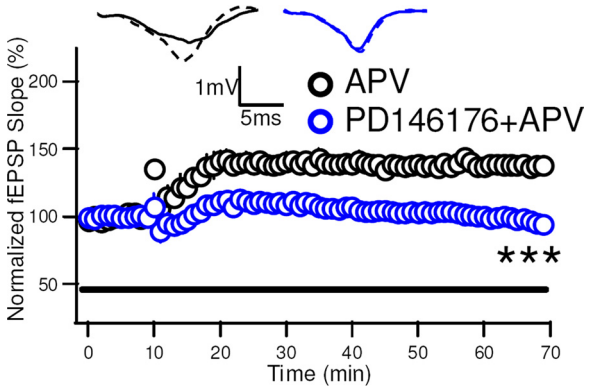


**Figure 4.** Pharmacological blockade of 12-LO abolishes LTCC-LTP. LTCC-dependent TBS-LTP in wild-type mice studied in the continuous presence of 50 μM D-APV was fully inhibited by 10 μM PD146176. Slices were preincubated in PD146716 for 2.5 h before experiment. Mean fEPSP amplitude was measured as percentage of baseline, averaged over a 5 min window 60 min after TBS. TBS in presence of D-APV (black) enhanced the fEPSP to 138 ± 3.45% of baseline ($n = 5$). In the presence of PD146176 plus D-APV (blue), TBS caused no significant change in fEPSP over baseline (96.6 ± 6.37%; $n = 6$; $p < 0.0005$ with unpaired Student's *t* test). The black bar indicates presence of drugs. Inset shows sample fEPSP traces before (solid line) and 60 min after (dashed line) LTP induction. Error bars represent ±SEM. The asterisks indicate significance level.

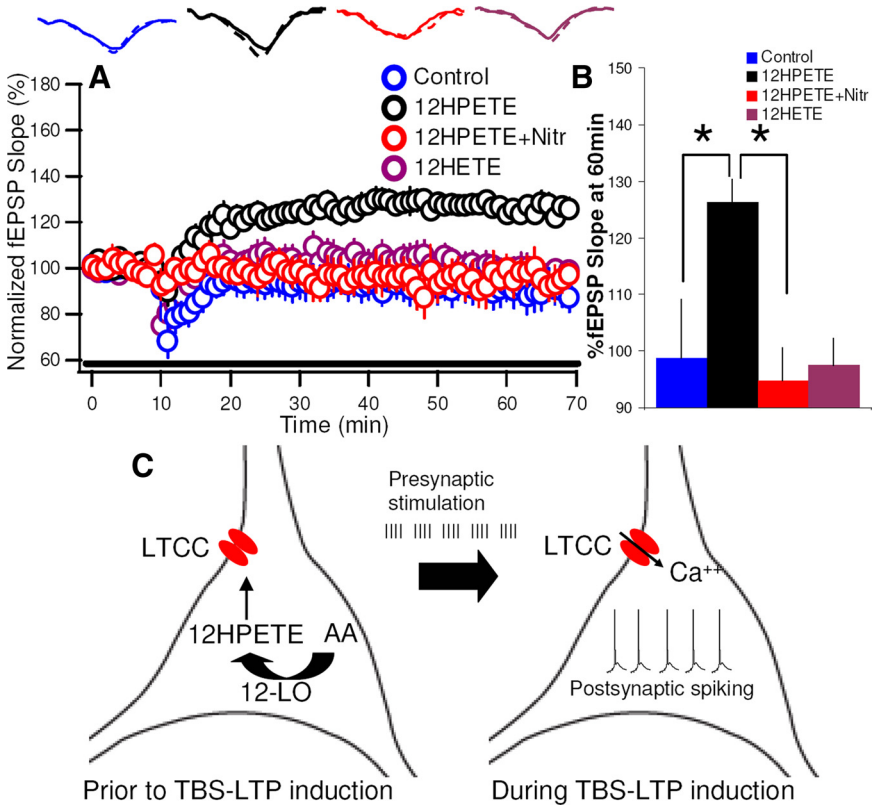


**Figure 5.** The 12-LO metabolite 12(*S*)-HPETE rescues LTCC-dependent LTP from pharmacological blockade of 12-LO. ***A***, Effects of application of 12-LO metabolites on induction of NMDAR-independent TBS-LTP in slices in which 12-LO was blocked by 10 $\mu$M PD146176 (PD). D-APV (50 $\mu$M) was also present to block NMDARs. Shown is the effect TBS delivered in the absence of 12(*S*)-HPETE (blue), in the presence of 250 nM 12(*S*)-HPETE (black), in the presence of 250 nM 12(*S*)-HPETE and 20 $\mu$M Nitr (red), and in the presence of 250 nM 12(*S*)-HETE (purple). The black bar indicates presence of drugs. Insets show sample fEPSP traces before (solid line) and 60 min after (dashed line) LTP induction. ***B***, Bar graph representing LTP measured as mean fEPSP during 5 min window 60 min after TBS expressed as percentage of baseline fEPSP before TBS. LTP was equal to 98.7 ± 10.4, 126.3 ± 3.96, 94.7 ± 5.9, and 97.5 ± 4.7% for control (no 12-LO metabolite) ($n = 6$), 250 nM 12(*S*)-HPETE ($n = 10$), 250 nM 12(*S*)-HPETE plus Nitr ($n = 5$), and 250 nM 12(*S*)-HETE ($n = 7$), respectively. Values of $p$ were 0.0147 for PD plus APV versus PD plus APV plus 12(*S*)-HPETE, 0.97 for PD plus APV versus PD plus APV plus 12(*S*)-HPETE plus Nitr, 0.99 for PD plus APV versus PD plus APV plus 12(*S*)-HETE, 0.0077 for PD plus APV plus 12(*S*)-HPETE versus PD plus APV plus 12(*S*)-HPETE plus Nitr. Comparisons were made with ANOVA and Tukey's *post hoc* test. Error bars represent ±SEM. The asterisks indicate significance level. ***C***, Model for 12-LO priming of induction of LTCC-dependent LTP. Basal 12-LO activity before TBS produces 12(*S*)-HPETE, thereby enabling LTCC activity and priming future induction of LTP. When TBS is applied, depolarization from postsynaptic spiking results in LTCC channel opening, and this $Ca^{2+}$ influx induces LTP.

These results suggest that 12(*S*)-HPETE may act upstream of the LTCC, perhaps by regulating LTCC activity and thus controlling $Ca^{2+}$ influx during theta burst stimulation.

The above data indicate that 12(*S*)-HPETE is an important 12-LO metabolite that mediates the positive regulatory effect on LTCCs, although the possible role of additional 12(*S*)-HPETE metabolites that have been noted in other systems (Piomelli et al., 1988; Piomelli et al., 1989) cannot be discounted. Our results further suggest that constitutive 12-LO activity generates levels of 12(*S*)-HPETE that prime LTCCs to provide sufficient $Ca^{2+}$ influx during TBS to induce LTP (Fig. 5*C*).

### $Ca^{2+}$ influx through L-type $Ca^{2+}$ channels during induction of LTP is impaired in 12-LO$^{-/-}$ mice

To explore directly the possibility that 12-LO activity is required for $Ca^{2+}$ influx, we measured the somatodendritic intracellular $Ca^{2+}$ transient elicited by the theta burst stimulation under control conditions and after blockade of 12-LO. CA1 pyramidal neurons were loaded with the $Ca^{2+}$-sensitive fluorescent dye Fluo-4 during whole-cell patch-clamp recordings and imaged using two-photon microscopy (Fig. 6*A*). A stimulus intensity was chosen such that a single burst of stimulation (five stimuli at 100 Hz) to the Schaffer collateral pathway yielded, on average, a single postsynaptic spike in the CA1 neuron. To minimize run-down of LTCC currents during whole-cell recording, the patch pipette was removed from the cell after 10 min of dye loading. This was followed by a 10 min recovery to preserve the function of LTCCs.

A single train of TBS applied to the Schaffer collateral pathway elicited postsynaptic spikes in the CA1 neuron that resulted in a clear fluorescence change, representing a rise in intracellular $Ca^{2+}$, in response to each burst during the train. We quantified the $Ca^{2+}$ signal by measuring the fluorescence change along a line scan through the proximal apical dendrite of a CA1 neuron, expressed as the change in fluorescence intensity divided by resting fluorescence (Fig. 6*A*, inset). Resting fluorescence was not different between genotypes, with 12-LO$^{+/+}$ neurons displaying a mean resting Fluo-4 fluorescence intensity of 71.5 ± 6.8 versus a value of 74 ± 8.1 in 12-LO$^{-/-}$ neurons ($p = 0.82$). The area under the line scan profile curve provided a measure of the time integral of the somatodendritic $Ca^{2+}$ signal elicited by a burst. This $Ca^{2+}$ signal in response to one train of TBS was similar between CA1 pyramidal neurons of 12-LO$^{-/-}$ and 12-LO$^{+/+}$ mice (Fig. 6*B*). Thus, a theta burst yielded a Ca integral of 27 ± 5.56% · s in 12-LO$^{+/+}$ mice ($n = 5$) and 24.2 ± 4.83% · s in neurons of 12-LO$^{-/-}$ mice ($n = 5$; $p = 0.71$). Despite this lack of overall change, the Nitr-sensitive component of the $Ca^{2+}$ signal was much reduced in the 12-LO$^{-/-}$ mice (Fig. 6*D*) compared with 12-LO$^{+/+}$ mice (Fig. 6*E*). In CA1 neurons from 12-LO$^{+/+}$ mice, Nitr blocked 58.8 ± 6.3% of the total TBS-induced Ca integral. In contrast, Nitr blocked only 23.5 ± 8.1% of the $Ca^{2+}$ integral in 12-LO$^{-/-}$ mouse pyramidal neurons ($p = 0.0063$). These data are thus consistent with the view that 12-LO is required for efficient $Ca^{2+}$ influx through L-type channels during theta burst stimulation.

### Whole-cell L-type $Ca^{2+}$ currents are reduced on blockade of 12-LO

Does 12-LO enhance $Ca^{2+}$ influx by directly regulating LTCC function or through an indirect effect, for example by affecting membrane excitability? A comparison of several whole-cell excitability parameters, including resting potential, input resistance, action potential threshold, and spike frequency revealed no significant differences between CA1 pyramidal neurons of 12-LO$^{-/-}$ and 12-LO$^{+/+}$ littermates (supplemental Fig. S2, Table S1, available at www.jneurosci.org as supplemental material). These results imply that 12-LO may have a direct regulatory effect on LTCC function.

To explore a possible direct effect of 12-LO on LTCC activity, we compared whole-cell $Ca^{2+}$ currents from CA1 pyramidal

neurons under voltage-clamp conditions in the presence and absence of PD146176. To isolate the $Ca^{2+}$ current, we blocked most voltage-gated potassium ($K^+$) channels by including cesium ($Cs^+$) in place of $K^+$ in the internal pipette solution and by including tetraethylammonium and 4-aminopyridine in the bath solution. Voltage-gated sodium ($Na^+$) channels were also inhibited with external TTX, and T-type calcium channels were inhibited with $Ni^{2+}$. Finally, to minimize contributions from T-type, N-type, and R-type voltage-gated $Ca^{2+}$ channels, which are also present in the postsynaptic somatodendritic compartment in addition to L-type channels, we held the membrane at a depolarized potential of −40 mV, a voltage at which these non-L-type channels are mostly inactivated. Under these conditions, $Ca^{2+}$ currents were determined in response to a series of 200-ms-long depolarizing voltage-clamp steps, and peak inward current was plotted as a function of test potential (Fig. 7).

The voltage steps elicited large net inward currents that increased in amplitude with increasing depolarization, reaching a peak inward value during steps to 0 mV. Application of Nitr caused a marked reduction in the peak current, from a value of 1151 ± 94 pA ($n = 14$) in the absence of drug to 671 ± 59 pA ($n = 18$) in the presence of Nitr ($p = 0.0012$). Thus, the Nitr-sensitive current, a measure of total L-type channel contribution, was equal to 480 pA, accounting for 42% of the total $Ca^{2+}$ current (Fig. 7*A*,*C*).

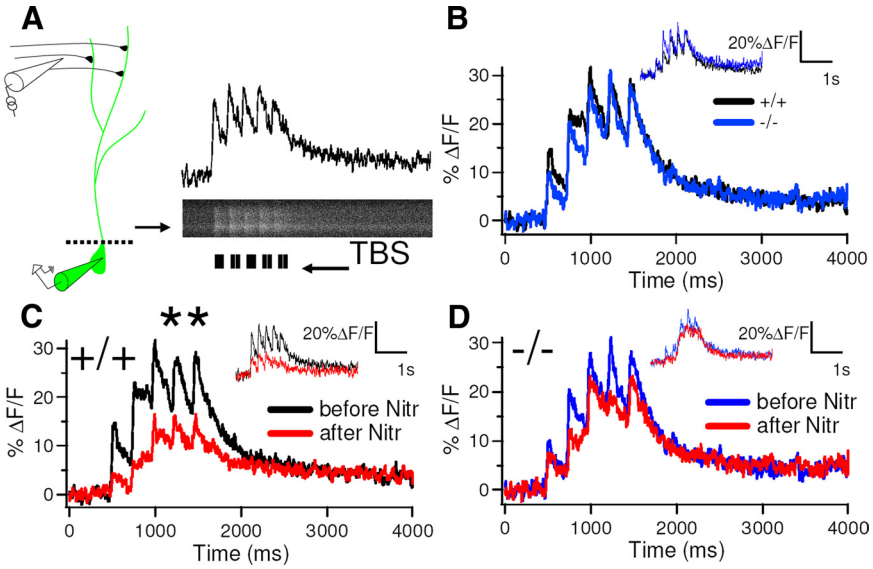


**Figure 6.** Somatodendritic $Ca^{2+}$ influx through LTCCs in response to a theta burst is impaired in CA1 pyramidal neurons of 12-LO $^{-/-}$ mice. The intracellular $Ca^{2+}$ signal in response to a theta burst stimulation was assessed with two-photon microscopy to determine the percentage of $Ca^{2+}$ influx entering through L-type $Ca^{2+}$ channels. ***A***, Schematic of experimental setup. CA1 pyramidal neurons were loaded with $Ca^{2+}$ dye using whole-cell patch recordings with a pipette filled with 200 $\mu$M Fluo-4. After dye loading, the patch pipette was removed from the cell to prevent extensive dialysis. The Schaffer collaterals were stimulated with a theta burst during line scan imaging across the proximal dendrite near the soma (dashed line). The inset shows a typical fluorescence trace in response to five bursts of stimuli at 5 Hz with each burst consisting of 10 spikes delivered at 100 Hz. Bottom, Raw line scan fluorescence. Top, Profile of average fluorescence signal across line during TBS. ***B***, Mean plots of $Ca^{2+}$ transient in response to TBS between 12-LO $^{+/+}$ (black; $n = 5$; black trace) and 12-LO $^{-/-}$ (blue; $n = 5$; blue trace) mice. $Ca^{2+}$ signal was calculated as area under the curves between 500 ms (start of TBS) to 2.5 s. TBS yielded an integral of 27 ± 5.56 s · % ($n = 5$) in CA1 neurons from 12-LO $^{+/+}$ mice versus 24.2 ± 4.83 s · % ($n = 5$) in neurons from 12-LO $^{-/-}$ mice ($p = 0.71$ with Student's unpaired *t* test). ***C***, Mean plots of $Ca^{2+}$ transient in CA1 neurons from 12-LO $^{+/+}$ mice before (black trace, $n = 5$) and after (red trace, $n = 5$) application of 20 $\mu$M Nitr. ***D***, Mean plots of $Ca^{2+}$ transient in CA1 neurons from 12-LO $^{-/-}$ pyramidal neurons before (blue trace; $n = 5$) and after (red trace; $n = 5$) 20 $\mu$M Nitr. Nitr blocked 58.8 ± 6.3% ($n = 5$) of the TBS-induced $Ca^{2+}$ signal in pyramidal neurons from wild-type mice versus 23.5 ± 8.1% ($n = 5$) in neurons from 12-LO $^{-/-}$ mice ($p = 0.0063$ with Student's unpaired *t* test). Insets show sample $Ca^+$ transients. The asterisks indicate significance level.

To examine the role of 12-LO in regulating LTCC current, we preincubated slices with 10 $\mu$M PD146176 and again measured $Ca^{2+}$ currents in the absence and presence of Nitr. The 12-LO blocker had no effect on the peak $Ca^{2+}$ current amplitude in the absence of Nitr, with a peak total $Ca^{2+}$ current equal to 1192 ± 142 pA ($n = 7$), similar to the total $Ca^{2+}$ current magnitude measured above in the absence of PD146176. However, preincubation with PD146176 greatly diminished the magnitude of the Nitr-sensitive current. Thus, in the presence of PD146176, Nitr reduced the $Ca^{2+}$ current only to 958 ± 98 pA ($n = 13$), a statistically insignificant change ($p = 0.99$), yielding a Nitr-sensitive current of 234 pA, approximately one-half the size of the current in the absence of the 12-LO inhibitor (Fig. 7*B*,*C*). These results demonstrate that, whereas the 12-LO inhibitor has no effect on the net $Ca^{2+}$ current, it does significantly reduce the L-type $Ca^{2+}$ channel current component, consistent with the effect that genetic deletion of 12-LO exerted on the $Ca^{2+}$ transient elicited by a burst of synaptic input. Possible reasons for why there is a lack of change in the total $Ca^{2+}$ signal or net $Ca^{2+}$ current despite the decrease in the LTCC-dependent component is discussed below.

## Discussion

This study establishes a role for 12-LO in long-term synaptic plasticity at CA3–CA1 synapses that is dependent on the pattern of tetanic stimulation used to induce the plastic changes. Thus, whereas NMDAR-dependent LTP induced by a 100 Hz tetanus is independent of 12-LO, LTCC-dependent LTP induced by 200 Hz tetanic stimulation does require this metabolic pathway. The physiological mechanism underlying this activity-dependent role of 12-LO results from its function to enable optimal $Ca^{2+}$ influx into the postsynaptic CA1 neuron through L-type $Ca^{2+}$ channels. Such channels appear to be recruited by theta burst patterns of activity (Fig. 3*A*) (Morgan and Teyler, 2001), but not by 100 Hz tetanic stimulation (supplemental Fig. S1, available at www.jneurosci.org as supplemental material), explaining the activity-dependent role of 12-LO. Moreover, the action of 12-LO appears to involve a direct modulatory effect on LTCC activity, rather than an indirect effect on action potential amplitude or duration, as pharmacological blockade of 12-LO reduces L-type current under voltage-clamp conditions (Fig. 7).

### Effects of 12-LO activity on L-type $Ca^{2+}$ channel function

One surprising result from our study is that genetic deletion of 12-LO or its pharmacological blockade reduced the Nitr-sensitive component of $Ca^{2+}$ influx measured either with a $Ca^{2+}$-sensitive dye or whole-cell voltage clamp but did not alter the net $Ca^{2+}$ signal or total $Ca^{2+}$ current. Although it is possible that loss of 12-LO activity simply reduces the sensitivity of the L-type channels to Nitr, such a change would have to be extremely large as we used suprasaturating concentrations of drug (20 $\mu$M; >100-fold greater than the $IC_{50}$). Moreover, a loss of Nitr

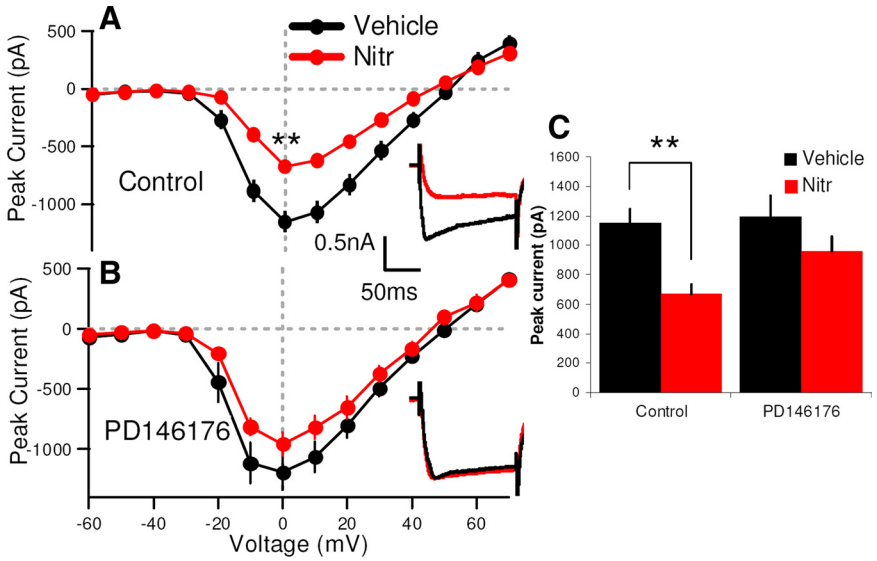


**Figure 7.** Pharmacological blockade of 12-LO reduces the macroscopic LTCC current in CA1 pyramidal neurons. ***A***, Whole-cell current–voltage relationships measured in the absence and presence of Nitr. Peak currents were measured for 200-ms-long voltage steps. Difference in curves in absence (black) and presence of Nitr (red) represents contribution of L-type $Ca^{2+}$ channels. Inset, Representative current traces shown during step to 0 mV. ***B***, Whole-cell current–voltage relationships in absence (black) and presence (red) of Nitr with 12-LO blocked in continuous presence of 10 $\mu$M PD146176. All measurements were performed in the presence of 0.05% DMSO, the solvent for Nitr. The inset depicts representative currents in the presence of PD146716 with and without Nitr. ***C***, Bar graph showing peak inward current of *I–V* plots in ***A*** and ***B*** during depolarization to 0 mV. Control, *I–V* data in absence of PD146176. Peak inward current was 1151 ± 94 pA in absence (black) of Nitr ($n = 14$) versus 671 ± 59 pA ($n = 18$) in presence (red) of Nitr ( $p = 0.00123$). PD146176, *I–V* data in presence of 12-LO inhibitor. Peak inward current was 1192 ± 142 pA in absence (black) of Nitr ($n = 7$) versus 958 ± 98 pA in presence (red) of Nitr ($n = 13$) ( $p = 0.564$). Comparisons are based on ANOVA with Tukey's *post hoc* comparison. Error bars represent ± SEM. The asterisks indicate significance level.

sensitivity alone cannot explain the effect of 12-LO knock-out or blockade to inhibit the LTCC-dependent component of TBS-LTP. Rather, the absence of an effect on net $Ca^{2+}$ current may result from homeostatic changes that upregulate other calcium channels, such as the N-type calcium channel, which is also present in the soma of CA1 pyramidal neurons. Alternatively, 12-LO activity may cause the tonic suppression of some other voltage-gated $Ca^{2+}$ channel. Nonetheless, any offsetting changes in $Ca^{2+}$ influx are insufficient to rescue NMDA receptor-independent LTP (Figs. 2, 4), indicating the privileged role that LTCCs must play in this form of plasticity.

A recent study used a hippocampus-restricted knock-out of the CaV1.2 LTCC isoform to demonstrate that this channel subtype underlies LTCC-dependent LTP at CA3–CA1 synapses (Moosmang et al., 2005). In contrast, genetic deletion experiments show that the CaV1.3 L-type isoform does not appear to be involved in LTP (Clark et al., 2003). This suggests that the CaV1.2 L-type channel provides the $Ca^{2+}$ source underlying LTCC-dependent LTP at CA3–CA1 synapses. Furthermore, our results indicate that it is the initial 12-LO metabolite of arachidonic acid, 12(*S*)-HPETE, rather than its more stable breakdown product, 12(*S*)-HETE, that is involved in LTCC-dependent LTP. Since LTCC function is required for certain forms of hippocampus-dependent learning (Borroni et al., 2000; Moosmang et al., 2005), 12-LO is likely a critical modulator of learning and memory.

### Role of 12-LO in the induction of LTCC-dependent LTP and other forms of plasticity

The above results suggest that LTCC function and TBS-LTP depend on levels of 12(*S*)-HPETE produced by 12-LO in response to low levels of synaptic activity. Evidence in support of the view that hippocampal neurons may produce basal levels of 12(*S*)-HPETE comes from the previous finding of our laboratories that even low-frequency (1 Hz) stimulation of CA3–CA1 Schaffer collaterals is able to generate significant levels of 12-LO metabolites of arachidonic acid (Feinmark et al., 2003). In this way, the role of 12-LO in the induction of LTP would represent a form of activity-dependent metaplasticity, similar to other forms of lipid-mediated metaplasticity (Fig. 5*C*) such as endocannabinoid-mediated metaplasticity, wherein the production of endocannabinoids during synaptic activity facilitates the subsequent induction of LTP at nearby synapses (Carlson et al., 2002; Chevaleyre and Castillo, 2004). Similarly, direct application of arachidonic acid to hippocampal slices facilitates induction of LTP by weak tetanic stimulation protocols that normally are insufficient to induce LTP (Williams et al., 1989; O'Dell et al., 1991). Interestingly, whereas we find that it is the 12-LO metabolites of arachidonic acid that are important for LTCC activation, arachidonic acid itself potentiates NMDA receptor currents (Miller et al., 1992). This suggests a divergent role in metaplasticity for the parent and daughter lipid metabolites, wherein each molecule primes a complementary $Ca^{2+}$ source for future induction of LTP.

12-LO metabolites of arachidonic acid have long been considered candidate retrograde messengers for LTP induction since they are cell permeant and they were shown to modulate glutamate release from presynaptic terminals in *Aplysia* sensory neurons (Piomelli et al., 1987a,b). However, the lack of specific pharmacological agents and the absence of a genetic knock-out impeded progress into understanding the role of 12-LO in LTP. Thus, early studies into the role of 12-LO in LTP gave inconclusive results, with some experiments indicating a reduction in basal transmission in the presence of a relatively nonspecific 12-LO inhibitor NDGA (nordihydroguaiaretic acid) (Williams and Bliss, 1988, 1989; Lynch et al., 1989), some indicating a block of LTP induction (Williams and Bliss, 1988, 1989; Lynch et al., 1989; O'Dell et al., 1991), and some indicating no effect on either basal transmission or LTP (Williams et al., 1989). It is noteworthy that these studies generally used 100 Hz tetanic stimulation rather than TBS for the induction of LTP, suggesting that LTCCs may not have been consistently recruited, perhaps accounting for the variable requirement for 12-LO.

Our combined results based on a genetic deletion of 12-LO and use of a selective 12-LO inhibitor help to define the discrete role of this enzyme in LTCC-dependent LTP. Although, as discussed above, the 12-LO metabolites are attractive candidates as retrograde signals, our results suggest that they are likely to play a different role, acting as priming signals to enable $Ca^{2+}$ influx into the postsynaptic cells in response to neural activity. Although such a result by itself does not rule out a second, presynaptic role of the metabolites, we found that application of 12(*S*)-HPETE, either alone or when paired with weak presynaptic activity, is insufficient to enhance synaptic transmission (supplemental Fig. S3*B*, available at www.jneurosci.org as supplemental material), arguing against its role as a retrograde signal in LTP.

Our finding that 12-LO and 12(*S*)-HPETE are required for LTCC-dependent LTP is of additional interest as this enzyme and metabolite are also required for induction of neonatal mGluR-dependent LTD (Feinmark et al., 2003), a form of long-term synaptic plasticity that is also LTCC dependent. Interestingly, application of 12(*S*)-HPETE is sufficient to induce a long-term decrease in synaptic transmission in the neonatal mice, in contrast to the lack of effect of the metabolite on basal transmission in the adult mice. Therefore, whereas 12-LO appears to be necessary and sufficient to mediate the expression of LTD in neonates, the enzyme is necessary but not sufficient to induce TBS-LTP in adults. Moreover, these results show that a single lipid metabolite can participate in opposing forms of plasticity, leading to either a decrease or increase in synaptic transmission, at distinct developmental stages.

### Comparison of effects of 12-LO metabolites on other ion channels

12-LO has been proposed to underlie several other neuromodulatory actions in other neurons and at other synapses, mainly through modulation of ion channels, including voltage-gated $Ca^{2+}$ channels, resting $K^+$ channels, and the TRPV family of vanilloid receptors. 12-LO has been suggested to modulate LTCC currents in growth cones to mediate turning induced by netrin-1 (Nishiyama et al., 2003). In *Aplysia* neurons, 12-LO and 12(*S*)-HPETE inhibit glutamate release at excitatory synapses and activate the serotonin-sensitive S-type $K^+$ channel. In mammals, 12-LO metabolites activate the two-pore TREK [two-pore domain weak inwardly rectifying $K^+$ channel (TWIK)-related $K^+$ channel] $K^+$ channels, which are thought to be closely related to the invertebrate S-type $K^+$ channels (Besana et al., 2005). 12-LO also may mediate opioid modulation of GABAergic (Vaughan et al., 1997) and glutamatergic transmission (Manzoni and Williams, 1999), perhaps by modulating a potassium current. The mechanism we describe here is distinct from these effects since 12-LO deletion did not alter baseline synaptic transmission, including paired-pulse ratio, emphasizing the selective role that 12-LO plays in the modulation of LTCCs in CA1 pyramidal neurons (Fig. 1*C*).

In addition to regulating $K^+$ channels, 12-LO metabolites regulate the endovanilloid receptor channel, TRPV1. Thus, in vertebrate sensory neurons, 12-LO appears to mediate the effects of histamine through the activation of TRPV1 (Shim et al., 2007). A recent study suggests that 12(*S*)-HPETE may mediate long-term depression at CA3 pyramidal neuron synapses onto CA1 inhibitory interneurons through activation of TRPV1 (Gibson et al., 2008). Notably, the LTP deficit described in the present study was independent of the presence of inhibitory synaptic transmission and so represents a distinct effect of 12-LO in regulating hippocampal plasticity (Fig. 2*B*).

12-LO, being membrane bound, is well poised to modulate ion channel function. Arachidonic acid and its metabolites, including lipoxygenase and cyclooxygenase products and endocannabinoids, represent a family of lipid mediators that play complementary roles in regulating synaptic function. In some cases, these molecules appear to provide an underlying tone to the system, thereby priming future signaling events such as synaptic plasticity. The importance of such metaplasticity in memory formation is emphasized by recent theoretical studies suggesting that metaplastic states are required to obtain sufficiently long memory lifetimes (Fusi et al., 2005; Fusi and Abbott, 2007). Future studies may define pathways that recruit or regulate 12-LO to dynamically control the ability to induce LTP during learning and memory.

## References


Besana A, Robinson RB, Feinmark SJ (2005) Lipids and two-pore domain $K^+$ channels in excitable cells. Prostaglandins Other Lipid Mediat 77:103–110.

Bliss TV, Collingridge GL, Morris RG (2003) Introduction. Long-term potentiation and structure of the issue. Philos Trans R Soc Lond B Biol Sci 358:607–611.

Borroni AM, Fichtenholtz H, Woodside BL, Teyler TJ (2000) Role of voltage-dependent calcium channel long-term potentiation (LTP) and NMDA LTP in spatial memory. J Neurosci 20:9272–9276.

Buttner N, Siegelbaum SA, Volterra A (1989) Direct modulation of *Aplysia* S-$K^+$ channels by a 12-lipoxygenase metabolite of arachidonic acid. Nature 342:553–555.

Carlson G, Wang Y, Alger BE (2002) Endocannabinoids facilitate the induction of LTP in the hippocampus. Nat Neurosci 5:723–724.

Cavuş I, Teyler T (1996) Two forms of long-term potentiation in area CA1 activate different signal transduction cascades. J Neurophysiol 76:3038–3047.

Chevaleyre V, Castillo PE (2004) Endocannabinoid-mediated metaplasticity in the hippocampus. Neuron 43:871–881.

Chevaleyre V, Takahashi KA, Castillo PE (2006) Endocannabinoid-mediated synaptic plasticity in the CNS. Annu Rev Neurosci 29:37–76.

Clark NC, Nagano N, Kuenzi FM, Jarolimek W, Huber I, Walter D, Wietzorrek G, Boyce S, Kullmann DM, Striessnig J, Seabrook GR (2003) Neurological phenotype and synaptic function in mice lacking the CaV1.3 alpha subunit of neuronal L-type voltage-dependent $Ca^{2+}$ channels. Neuroscience 120:435–442.

Collingridge GL (2003) The induction of *N*-methyl-D-aspartate receptor-dependent long-term potentiation. Philos Trans R Soc Lond B Biol Sci 358:635–641.

Collingridge GL, Kehl SJ, McLennan H (1983) Excitatory amino acids in synaptic transmission in the Schaffer collateral-commissural pathway of the rat hippocampus. J Physiol 334:33–46.

Feinmark SJ, Begum R, Tsvetkov E, Goussakov I, Funk CD, Siegelbaum SA, Bolshakov VY (2003) 12-Lipoxygenase metabolites of arachidonic acid mediate metabotropic glutamate receptor-dependent long-term depression at hippocampal CA3–CA1 synapses. J Neurosci 23:11427–11435.

Fusi S, Abbott LF (2007) Limits on the memory storage capacity of bounded synapses. Nat Neurosci 10:485–493.

Fusi S, Drew PJ, Abbott LF (2005) Cascade models of synaptically stored memories. Neuron 45:599–611.

Gibson HE, Edwards JG, Page RS, Van Hook MJ, Kauer JA (2008) TRPV1 channels mediate long-term depression at synapses on hippocampal interneurons. Neuron 57:746–759.

Grover LM, Teyler TJ (1990) Two components of long-term potentiation induced by different patterns of afferent activation. Nature 347:477–479.

Johnston D, Williams S, Jaffe D, Gray R (1992) NMDA-receptor-independent long-term potentiation. Annu Rev Physiol 54:489–505.

Kitamura S, Shimizu T, Izumi T, Seyama Y (1987) Synthesis of 11,12-leukotriene A4, 11*S*,12*S*-oxido-5*Z*,7*E*,9*E*,14*Z*-eicosatetraenoic acid, a novel leukotriene of the 12-lipoxygenase pathway. FEBS Lett 213:169–173.

Lamsa K, Heeroma JH, Kullmann DM (2005) Hebbian LTP in feed-forward inhibitory interneurons and the temporal fidelity of input discrimination. Nat Neurosci 8:916–924.

Lynch MA, Errington ML, Bliss TV (1989) Nordihydroguaiaretic acid blocks the synaptic component of long-term potentiation and the associated increases in release of glutamate and arachidonate: an in vivo study in the dentate gyrus of the rat. Neuroscience 30:693–701.

Malenka RC, Bear MF (2004) LTP and LTD: an embarrassment of riches. Neuron 44:5–21.

Manzoni OJ, Williams JT (1999) Presynaptic regulation of glutamate release in the ventral tegmental area during morphine withdrawal. J Neurosci 19:6629–6636.

Miller B, Sarantis M, Traynelis SF, Attwell D (1992) Potentiation of NMDA receptor currents by arachidonic acid. Nature 355:722–725.

Moosmang S, Haider N, Klugbauer N, Adelsberger H, Langwieser N, Müller J, Stiess M, Marais E, Schulla V, Lacinova L, Goebbels S, Nave KA, Storm DR, Hofmann F, Kleppisch T (2005) Role of hippocampal Cav1.2 $Ca^{2+}$ channels in NMDA receptor-independent synaptic plasticity and spatial memory. J Neurosci 25:9883–9892.

Morgan SL, Teyler TJ (1999) VDCCs and NMDARs underlie two forms of LTP in CA1 hippocampus in vivo. J Neurophysiol 82:736–740.

Morgan SL, Teyler TJ (2001) Electrical stimuli patterned after the theta-rhythm induce multiple forms of LTP. J Neurophysiol 86:1289–1296.

Nishiyama M, Hoshino A, Tsai L, Henley JR, Goshima Y, Tessier-Lavigne M, Poo MM, Hong K (2003) Cyclic AMP/GMP-dependent modulation of $Ca^{2+}$ channels sets the polarity of nerve growth-cone turning. Nature 423:990–995.

O'Dell TJ, Hawkins RD, Kandel ER, Arancio O (1991) Tests of the roles of two diffusible substances in long-term potentiation: evidence for nitric oxide as a possible early retrograde messenger. Proc Natl Acad Sci U S A 88:11285–11289.

Piomelli D, Volterra A, Dale N, Siegelbaum SA, Kandel ER, Schwartz JH, Belardetti F (1987a) Lipoxygenase metabolites of arachidonic acid as second messengers for presynaptic inhibition of *Aplysia* sensory cells. Nature 328:38–43.

Piomelli D, Shapiro E, Feinmark SJ, Schwartz JH (1987b) Metabolites of arachidonic acid in the nervous system of *Aplysia*: possible mediators of synaptic modulation. J Neurosci 7:3675–3686.

Piomelli D, Feinmark SJ, Shapiro E, Schwartz JH (1988) Formation and biological activity of 12-ketoeicosatetraenoic acid in the nervous system of *Aplysia*. J Biol Chem 263:16591–16596.

Piomelli D, Shapiro E, Zipkin R, Schwartz JH, Feinmark SJ (1989) Formation and action of 8-hydroxy-11,12-epoxy-5,9,14-icosatrienoic acid in *Aplysia*: a possible second messenger in neurons. Proc Natl Acad Sci U S A 86:1721–1725.

Sendobry SM, Cornicelli JA, Welch K, Bocan T, Tait B, Trivedi BK, Colbry N, Dyer RD, Feinmark SJ, Daugherty A (1997) Attenuation of diet-induced atherosclerosis in rabbits with a highly selective 15-lipoxygenase inhibitor lacking significant antioxidant properties. Br J Pharmacol 120:1199–1206.

Shim WS, Tak MH, Lee MH, Kim M, Kim M, Koo JY, Lee CH, Kim M, Oh U (2007) TRPV1 mediates histamine-induced itching via the activation of phospholipase A2 and 12-lipoxygenase. J Neurosci 27:2331–2337.

Striessnig J, Koschak A, Sinnegger-Brauns MJ, Hetzenauer A, Nguyen NK, Busquet P, Pelster G, Singewald N (2006) Role of voltage-gated L-type $Ca^{2+}$ channel isoforms for brain function. Biochem Soc Trans 34:903–909.

Sun D, Funk CD (1996) Disruption of 12/15-lipoxygenase expression in peritoneal macrophages. Enhanced utilization of the 5-lipoxygenase pathway and diminished oxidation of low density lipoprotein. J Biol Chem 271:24055–24062.

Vaughan CW, Ingram SL, Connor MA, Christie MJ (1997) How opioids inhibit GABA-mediated neurotransmission. Nature 390:611–614.

Williams JH, Bliss TV (1988) Induction but not maintenance of calcium-induced long-term potentiation in dentate gyrus and area CA1 of the hippocampal slice is blocked by nordihydroguaiaretic acid. Neurosci Lett 88:81–85.

Williams JH, Bliss TV (1989) An in vitro study of the effect of lipoxygenase and cyclo-oxygenase inhibitors of arachidonic acid on the induction and maintenance of long-term potentiation in the hippocampus. Neurosci Lett 107:301–306.

Williams JH, Errington ML, Lynch MA, Bliss TV (1989) Arachidonic acid induces a long-term activity-dependent enhancement of synaptic transmission in the hippocampus. Nature 341:739–742.

Zakharenko SS, Zablow L, Siegelbaum SA (2001) Visualization of changes in presynaptic function during long-term synaptic plasticity. Nat Neurosci 4:711–717.

Zakharenko SS, Patterson SL, Dragatsis I, Zeitlin SO, Siegelbaum SA, Kandel ER, Morozov A (2003) Presynaptic BDNF required for a presynaptic but not postsynaptic component of LTP at hippocampal CA1-CA3 synapses. Neuron 39:975–990.